Transport and Anisotropic Diffusion in Time-Dependent Flow Visualization

D. Bürkle* T. Preußer† M. Rumpf†

Abstract

The visualization of time-dependent flow is an important and challenging topic in scientific visualization. Its aim is to represent transport phenomena governed by time-dependent vector fields in an intuitively understandable way, using images and animations. Here we pick up the recently presented anisotropic diffusion method, expand and generalize it to allow a multiscale visualization of long-time, complex transport problems. Instead of streamline type patterns generated by the original method now streakline patterns are generated and advected. This process obeys a nonlinear transport diffusion equation with typically dominant transport. Starting from some noisy initial image, the diffusion actually generates and enhances patterns which are then transported in the direction of the flow field. Simultaneously the image is again sharpened in the direction orthogonal to the flow field. A careful adjustment of the modelś parameters is derived to balance diffusion and transport effects in a reasonable way. Properties of the method can be discussed for the continuous model, which is solved by an efficient upwind finite element discretization. As characteristic for the class of multiscale image processing methods, we can in advance select a suitable scale for representing the flow field.

Keywords: flow visualization, multiscale image processing, nonlinear diffusion, transport diffusion, upwind method

1 Introduction

Time-dependent flow is still one of the challenging topics concerning its efficient computation as well as its effective visualization. The typically different local scales in a single data set and the fact that the motion itself is related to an integration of the given velocity field rather than to the field itself had stimulated many different solution strategies.

In the last decade various methods for the visualization of flow fields and interesting flow features have been presented. The spot noise method proposed by van Wijk [17] and its later extension [5, 18] uses a blending of many spot like texture splats aligned by deformation to the velocity field in 2D or on surfaces in 3D. The Line Integral Convolution (LIC) approach of Cabral and Leedom [4] integrates a white noise along particle lines making use of the accompanying strong correlation of the resulting intensities along streamlines. This method has been extended in various directions [16, 6]. Other texture based methods are discussed by Max et al. [9], Max and Becker [8], Becker and Rumpf [3]. Weinstein et al. [20] have presented a method for advection diffusion based propagation through tensor fields.

Most of the methods presented so far have in common, that the generation of a coarser scale requires a re-computation. Time-dependent flow fields, which will be our main focus here, have been discussed in [15, 9, 3] and an animated version of LIC is given by Shen and Kao [15]. For further references we refer to [13] and the bibliography given there.

Here, we will extend previous work [13] on image processing methodology applied to the visualization of flow fields. This method was based on the solution of an anisotropic diffusion problem with an anisotropy strongly aligned to the flow field. Diffusion type methods are popular methods in image processing and go back to the early work of Perona and Malik [10]. Theoretically this class of methods has been studied by Alvarez, Guichard, Lions and Morel [1], Kawohl and Kutev [2], and others. Anisotropic diffusion was introduced by Weickert [19]. Appropriate finite element discretization and its convergence properties have been studied by Kačur and Mikula [7].

Now, for time-dependent flow fields we generate a flow aligned texture, which moves continuously with the flow. Especially in an animation, the underlying transport will intuitively be visualized on a previously selected scale of resolution. Thus, instead of a diffusion problem we now solve a transport diffusion equation. The equation models the underlying motion and the diffusion together with a suitable source term on the right hand side. This leads to the generation of a flow aligned pattern. Qualitative properties of the method are studied on the level of the continuous model. Finally, a finite element discretization in space and a semi implicit upwind scheme in time are applied to solve this problem numerically.

2 Reviewing the Anisotropic Diffusion Method

In [13] a method based on anisotropic diffusion is presented which allows to build a texture representing a given steady state flow field globally on the spatial domain. This method, which will be briefly reviewed in this section, generates streamline like patterns and in addition carries the possibility to successively coarsen those patterns. Thereby we pick up the line integral convolution (LIC) approach as proposed by Cabral and Leedom [4] using the observation that the built in convolution along streamlines corresponds to solving the heat equation on the streamlines. The desired coarsening will be steered by a Perona Malik [11] type diffusion that acts in the direction orthogonal to the flow field.

To be more precise, let $v : \Omega \to \mathbb{R}^d$ be a given vector field on a domain Ω , which we assume to be continuous and non vanishing on Ω. Clearly there exists a family of orthogonal mappings $B(x) : \Omega \to SO(n)$ such that $B(x)v(x) = e_0$, where $\{e_i\}_{i=0,\cdots,d-1}$ is the standard basis in $\mathbb{R}^d$. Hence, we consider a diffusion tensor $A(\nabla\rho_\sigma)$ depending on the vector field v defined by

$$A(v, \nabla\rho_\sigma) = B(x)^T \begin{pmatrix} \alpha(\|v(x)\|) & 0 \\ 0 & G(\|\nabla\rho_\sigma\|)\,\mathrm{Id}_{d-1} \end{pmatrix} B(x),$$

with e.g.

$$G(s) = \frac{1}{1 + s^2/\lambda^2}, \qquad \lambda \in \mathbb{R},$$

and solve the parabolic boundary initial value problem

$$\partial_t \rho + \nabla\rho \cdot v - \mathrm{div}\,(A(v, \nabla\rho_\epsilon)\nabla\rho) = f(\rho)$$

*Institut für Angewandte Mathematik, Freiburg University, Hermann-Herder-Str. 10, 76104 Freiburg, Germany, *buerkle@math.uni-freiburg.de*

†Fachbereich Mathematik, Duisburg University, Lotharstraße 65, 47048 Duisburg, Germany, *[preusser, rumpf]@math.uni-duisburg.de*

in $\mathbb{R}^+ \times \Omega$ with Neumann boundary conditions prescribed on $\partial\Omega$ and some white noise ρ_0 as initial data at time $t = 0$. The coefficient $\alpha : \mathbb{R}^+ \to \mathbb{R}^+$ controls the linear diffusion in vector field direction, i. e. along streamlines, and the edge enhancing diffusion coefficient $G(\cdot)$ acts in the orthogonal directions. In general, we choose α to be a constant function, but we may also select a monotone function with $\alpha(0) > 0$ and $\lim_{\alpha\to\infty} \alpha(s) = \alpha_{\max}$. During the evolution, patterns will diffuse along the streamlines, but there is still some diffusion perpendicular to the flow field. This supplies us with coarser representations of the flow field as the scale increases. Unfortunately, if we run the evolution with a vanishing right hand side f, the contrast of the image density will decrease, because of the linear diffusion along streamlines. Thus, we select a source term $f : [0,1] \to \mathbb{R}^+$ satisfying

$$\begin{aligned} f(0) = 0, \quad f < 0 \quad &\text{on } (0, 0.5), \\ f(1) = 0, \quad f > 0 \quad &\text{on } (0.5, 1), \end{aligned} \tag{1}$$

that pushes values toward zero and 1, respectively. A well known maximum principle ensures that we do not enlarge the interval of gray values using this f. Choosing am m dimensional vector valued diffusion with $m \in \{2, 3\}$ instead of a scalar diffusion provides additional asymptotic states of the process. We then select the corresponding initial data randomly distributed within the cube $[0,1]^m$, interpret the components of ρ as color-components and define the force f to work on the luminance of ρ. In Figures 1 and 2 we have depicted scales of vector field representations. For details we refer to the original paper [13].

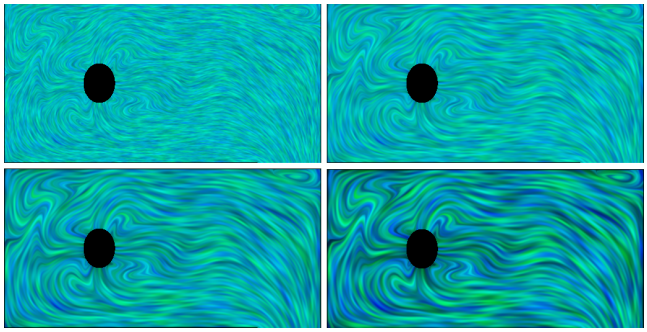

Figure 1: From top left to bottom right four successive scale steps of the anisotropic diffusion process are depicted. The vector field visualized here results from a CFD computation, where a fluid flows from the inlet (black circle) toward an outlet on the lower right corner.

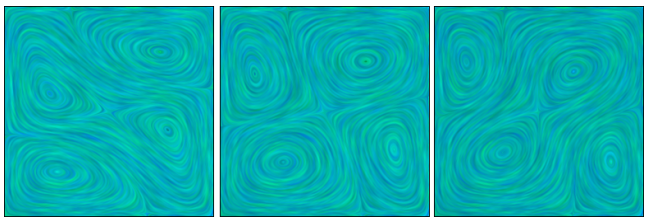

Figure 2: Three different time-steps of a convective flow visualized by the anisotropic diffusion method for steady flow fields, which nicely represent the vector fields but not the underlying time-dependent motion. Thereby, the resulting pattern is directed along streamlines. Cf. Fig. 6 for streakline type pattern generated by the new transport diffusion method corresponding to the same time-steps.

3 A Transport Diffusion Model

The above reviewed anisotropic diffusion method generates streamline type patterns, which are aligned to trajectories of the vector field for a fixed given time. I. e. for a time-dependent vector field $v : \mathbb{R}^+ \times \Omega \to \mathbb{R}^d$ on a computational domain $\Omega \subset \mathbb{R}^d$ and $d = 2, 3$, we consider integral lines $\{x(s) \,|\, s \in \mathbb{R}\}$ with $\frac{d}{ds}x(s) = v(t, x(s))$ for fixed t. Thus, the method intuitively visualizes the vector field freezed at time t but offers only very limited insight in the actual transport process governed by the underlying time-dependent flow field.

To ensure that our visualization actually displays this process we have to consider the true transport problem and its particle lines respectively. Hence we take into account the particle motion obeying the equation $\frac{d}{dt}x(t) = v(t, x(t))$ and the induced transport of a given density $\rho(t, x)$. Due to the fact that such a purely advected density ρ stays constant along particle trajectories, i. e. $\frac{d}{dt}\rho(t, x(t)) = (\frac{\partial}{\partial t}\rho + \nabla\rho \cdot v)(t, x(t))$ we finally obtain as a conservation law the vanishing of the material derivative

$$\frac{D}{dt}\rho := \frac{\partial}{\partial t}\rho + \nabla\rho \cdot v = 0\,.$$

The material derivative will later play a crucial role concerning our choice for a proper discretization. Furthermore, we have to incorporate a mechanism for the generation, the growth and enhancement of flow aligned patterns. Here we pick up the previous model and consider a simultaneous anisotropic nonlinear diffusion process with linear diffusion along the particle line and sharpening in the perpendicular direction. Let us emphasize here, that this diffusion process acts in forward *and* backward direction of the particle line. Thus, a careful control of the parameters is indispensable to avoid an artificial propagation in downwind direction with the accompanying visual impression of a wrong velocity. In Section 4 we will discuss in detail a suitable balance of parameters and in Section 5 a modified approach will be presented which copes with this problem in a slightly different way.

Finally, our basic *transport diffusion* model for time-dependent vector fields looks as follows: On the computational domain $\Omega \subset \mathbb{R}^d$ we consider for a given vector field $v : \mathbb{R}^+ \times \Omega \to \mathbb{R}^d$ the boundary and initial value problem:

$$\begin{aligned} \partial_t\rho + \nabla\rho \cdot v - \operatorname{div}\left(A(v, \nabla\rho_\epsilon)\nabla\rho\right) &= f(\rho) && \text{in } \mathbb{R}^+ \times \Omega, \\ (A\nabla\rho) \cdot \nu &= 0 && \text{on } \mathbb{R}^+ \times \partial\Omega, \\ \rho(0, \cdot) &= \rho_0 && \text{in } \Omega, \end{aligned}$$

where $A(v, \nabla\rho_\epsilon)$ is the diffusion tensor already known from the anisotropic diffusion for steady flow fields

$$A(v, \nabla\rho_\epsilon) = B(x)^T \begin{pmatrix} \alpha(\|v\|) & 0 \\ 0 & G(\nabla\rho_\epsilon \cdot v)\mathrm{Id}_{d-1} \end{pmatrix} B(x),$$

in the flow aligned coordinate system. Initial data ρ_0 is again assumed to be a white noise of appropriate frequency. Still the role of the right hand side f is to ensure contrast enhancement. Thus we assume functions f which fulfill the properties mentioned in Section 2.

The new model generates and stretches patterns along the flow field and transports them simultaneously. The resulting motion texture is characterized by a dense coverage of the domain with streakline type patterns, which do not have a fixed injection point but move in time with the fluid (cf. Figures 3 and 6). At least at the head of the patterns the enhancement direction is orthogonal to the stretching direction of the corresonding streaklines.

In case of inflow boundary conditions we have to ensure the same scale of patterns close to the inflow. Unfortunately, such a pattern needs to be transported into the domain from outside. Therefore we

enlarge the computational domain, extrapolate the velocity, compute the transport diffusion problem and finally extract a region of interest from the enlarged computational domain.

As already mentioned in the introduction, the new model comes along with an image processing multiscale of successively sharper and coarser images in time – typically represented by a separate time in the corresponding diffusion problem – and the actual time corresponding to the underlying transport process. Fixing the process time and varying the scale we are back at the original anisotropic diffusion method for steady vector fields. Identifying process time and scale parameter - as we propose here - we end up with a pattern advection method but the resulting images correspond to successively coarser scales. The ideal case would be to fix the scale and vary the process time only. Unfortunately this is not possible within the scope of our method. Nevertheless we can prescribe a suitable scale interval and apply a blending technique, where we select from different transport diffusion problems with temporal overlap always those, which correspond to a given scale range. Compare Section 7 for details.

4 Balancing Parameters

In general, transport and diffusion are contrary processes. Our goal in mind – the generation and transport of patterns which simultaneously diffuse along the flows, there has to be a careful weighting of the parameters that steer the transport and the diffusion respectively. Otherwise the diffusion may overrun the transport, resulting in a process that is rather diffusion than transport with some pattern generating diffusion.

It is well known that the solution of the heat equation at a time t corresponds to the convolution of the initial data with a Gaussian kernel of variance $\sqrt{2t}$. Since the diffusion tensor $A(v)$ invokes linear diffusion with a coefficient $\alpha(\|v(x)\|)$ in the direction of the velocity $v(x)$ for every $x \in \Omega$, we consider the corresponding variance

$$\mathcal{D}(\alpha(x)) := \sqrt{2\tau\alpha(x)}$$

to be a measure for the diffusion within the transport diffusion process for a time-step τ. Of course a measure for the corresponding expected transport distance is

$$\mathcal{T}(x) := \tau\|v(x)\|.$$

Typically $\mathcal{T}(\cdot)$ is more or less fixed, since τ is usually prescribed by the underlying CFD data. Thus, we would like to adjust α locally such that $\mathcal{D}$ is balanced with $\mathcal{T}$. To this end we introduce a balancing parameter $\beta \in \mathbb{R}^+$ and consider the balancing condition

$$\mathcal{D}(\alpha(x)) = \beta\mathcal{T}(x).$$

Roughly speaking we then have the following relations:

$\beta \ll 1$	Transport dominates the model,
$\beta = 1$	Transport $\approx$ Diffusion,
$\beta \gg 1$	Diffusion dominates the model.

Hence, choosing $\beta < 1$ fixed, and solving the balance condition for $\alpha(x)$, we get a suitable diffusion coefficient

$$\alpha(\|v\|)(x) = \frac{\beta^2\|v(x)\|^2\tau}{2}$$

as a function on the domain Ω which is inserted into the diffusion tensor A of our transport diffusion model.

Furthermore, let us study the amplification of certain frequencies of the initial image due to the right hand side of our model. Our focus will be on the influence of the shape of $f(\cdot)$ on the constrast enhancing property of the model. To this end let us consider a much simpler setting of a high frequency initial data given by

$$u_0(x) = \frac{1}{2}\left[\sin\left(\frac{x}{\epsilon}\right) + 1\right]$$

and restrict ourselves to a simple diffusion equation along a (1-dimensional) streamline, which is given by

$$\partial_t u - \alpha\Delta u = f(u) \qquad \text{in } [0,1].$$

Let us linearize f around $\frac{1}{2}$ and consider

$$\tilde{f}(u) = \gamma(u - \frac{1}{2}),$$

where γ is the slope of the original f at $\frac{1}{2}$. Taking into account the ansatz $u(t) = a(t)\left(u_0(x) - \frac{1}{2}\right) + \frac{1}{2}$, we get

$$\frac{1}{2}\left[a' + \left(\frac{\alpha}{\epsilon^2} - \gamma\right)a\right]\sin\left(\frac{x}{\epsilon}\right) = 0$$

and so $a(t) = \exp\left[\left(\gamma - \frac{\alpha}{\epsilon^2}\right)t\right]$. This means that frequencies above $\sqrt{\frac{\alpha}{\gamma}}$ are damped, whereas frequencies below this threshold are amplified. Given an upper threshold $\frac{1}{\epsilon}$ for the frequencies which we want to amplify, we choose

$$\gamma = \frac{\alpha}{\epsilon^2}.$$

Finally, we construct our nonlinear right hand side $f(\cdot)$ in such a way that the slope at $\frac{1}{2}$ equals γ (cf. Fig. 4).

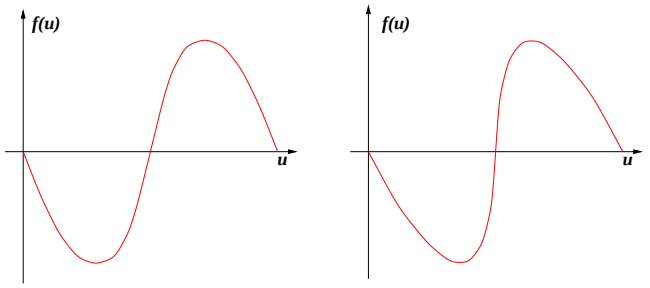

Figure 4: Source terms with different slopes at $\frac{1}{2}$, which are applied to amplify different frequency ranges in the evolution.

5 Generating directed patterns

The above discussed balancing of parameters with respect to a dominated transport does not completely diminish diffusion effects downstream. At least at the head of the evolving pattern a slight modification of the proposed model helps to avoid this misleading drawback. Hence, we incorporate a "one–sided" diffusion related to our model for flow segmentation [13]. I. e. we replace the tangential diffusivity $\alpha(v)$ by

$$\alpha(v, \nabla\rho) = \begin{cases} \alpha_{\max}\, G\left((\nabla\rho \cdot v)_+\right) & \text{if } \rho \le 0.5, \\ \alpha_{\max} & \text{else,} \end{cases}$$

which depends in addition on the evolving intensity. Then lighter pattern will not diffuse downstream and a sharp front at the tip of the pattern together with a typically blurred intensity in the upstream direction will underline the direction of the flow (cf. Fig. 5).

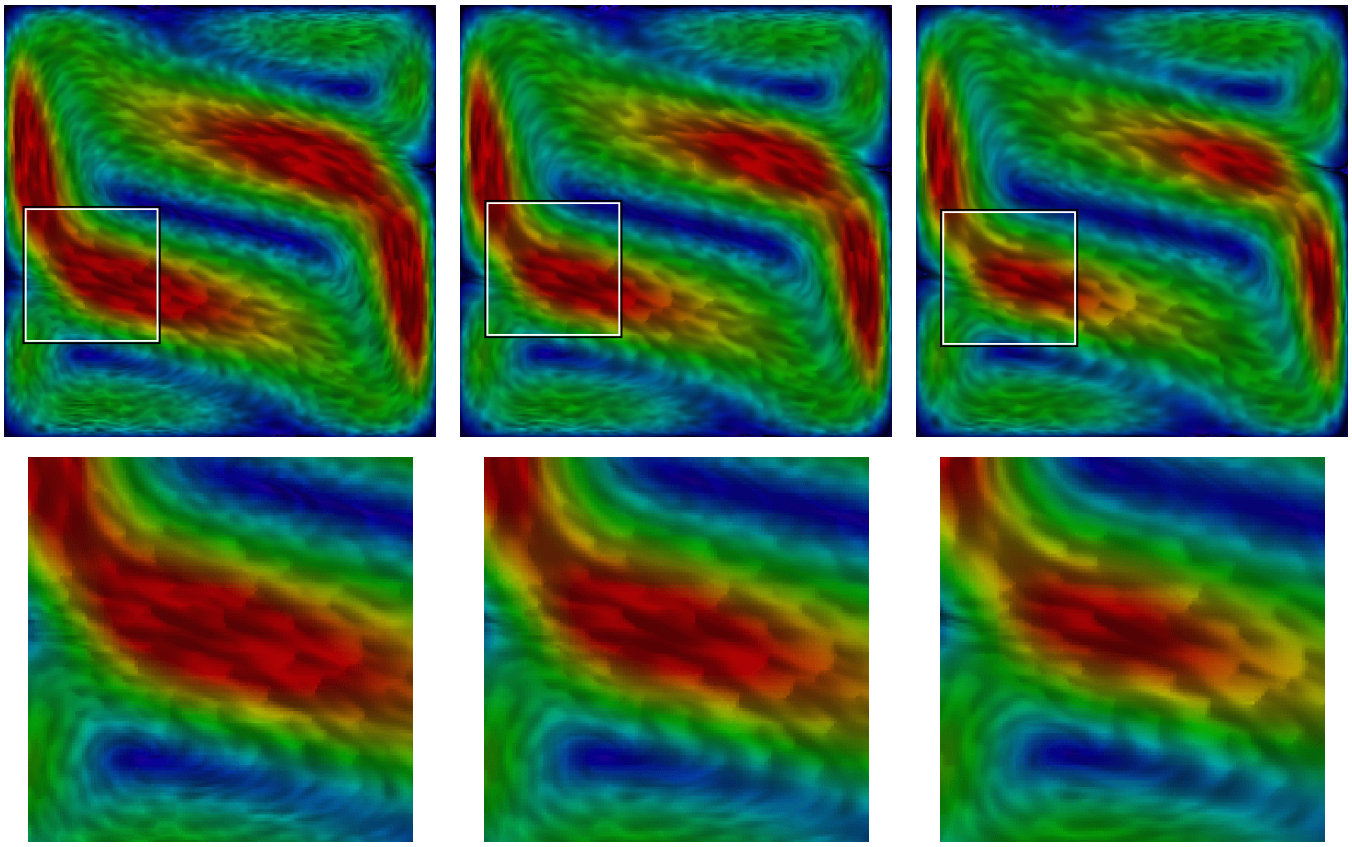

Figure 3: Three successive time-steps of the transport diffusion process generating directed patterns of a Bénard convection (cf. Section 5). The additional coloring indicates the speed of the flow field. Red colors indicate high velocity, whereas blue colors indicate low velocity. To emphasize the transport of patterns we have magnified the marked sections of the images in the lower row.

6 Discretization

For the discretization of the above transport diffusion problem we pick up an algorithm due to Pironneau [12] for the discretization of transport dominated problem. Furthermore, for the diffusive term of the equation we apply a semi-implicit scheme, where the diffusion coefficient $G(\cdot)$ and the right hand side $f(\cdot)$ are evaluated at the previous time-step. Let us indicate by an upper index n the time-step and by τ the time-step size. Then, a suitable approximation of the material derivative at time $t_n = n\,\tau$ is given by

$$\frac{D}{dt}\rho(t_n,\cdot) \approx \frac{\rho^{n+1} - \rho^n \circ X^n}{\tau},$$

where X^n is a numerical upwind integration of the velocity field, i. e. $X^n(x) \approx x(t_n)$ with $\dot{x}(t) = v(t, x(t))$ and $x(t_{n+1}) = x$. We consider the following second order approximation:

$$X^n(x) = x - \tau v\left(t_{n+1} - \frac{\tau}{2},\, x - \frac{\tau}{2} v(t_{n+1}, x)\right)$$

Next, following Pironneau we incorporate this approximation of the transport into a variational formulation of the transport diffusion problem and obtain:

$$\left(\frac{\rho^{n+1} - \rho^n \circ X^n}{\tau}, \theta\right) + \left(A(v, \nabla\rho_\epsilon^n \circ X^n)\nabla\rho^{n+1}, \nabla\theta\right) = \left(f(\rho^n \circ X^n), \theta\right) \qquad \forall\theta \in C^\infty(\Omega),$$

where $(\cdot,\cdot)$ denotes the L^2 scalar product on Ω. Finally, from this variational formulation a spatial finite element discretization can be easily derived. I. e. in 2D we consider bilinear finite elements on a regular grid and lumped mass integration. As proposed in the original anisotropic diffusion method for steady flow fields the same regularized ρ_ϵ is considered in each time-step based on a single short implicit time-step for the corresponding heat equation with respect to initial data ρ.

7 A Blending Strategy for Long-Term Animation

One of the characteristics of nonlinear diffusion methods in image processing is that the corresponding evolution generates a scale of representations, ranging from fine and typically noisy to coarse images with enhanced features such as edges. We have observed this scale of representations already in the anisotropic diffusion method for steady flow fields. As proposed above, the scale parameter is now coupled to the actual transport process in our transport diffusion model. But especially for long-term visualization purposes this coupling obviously leads to non satisfying results. Unfortunatly, due to the nature of our model, we are unable to freeze the scale and solely consider the evolution of suitable patterns at that specific scale in time, which would be the optimal choice. The solution we propose here is a compromise based on the blending of different results from the transport diffusion evolution started at successively incremented times.

Fig. 7 gives a sketch of the different approaches in a diagram

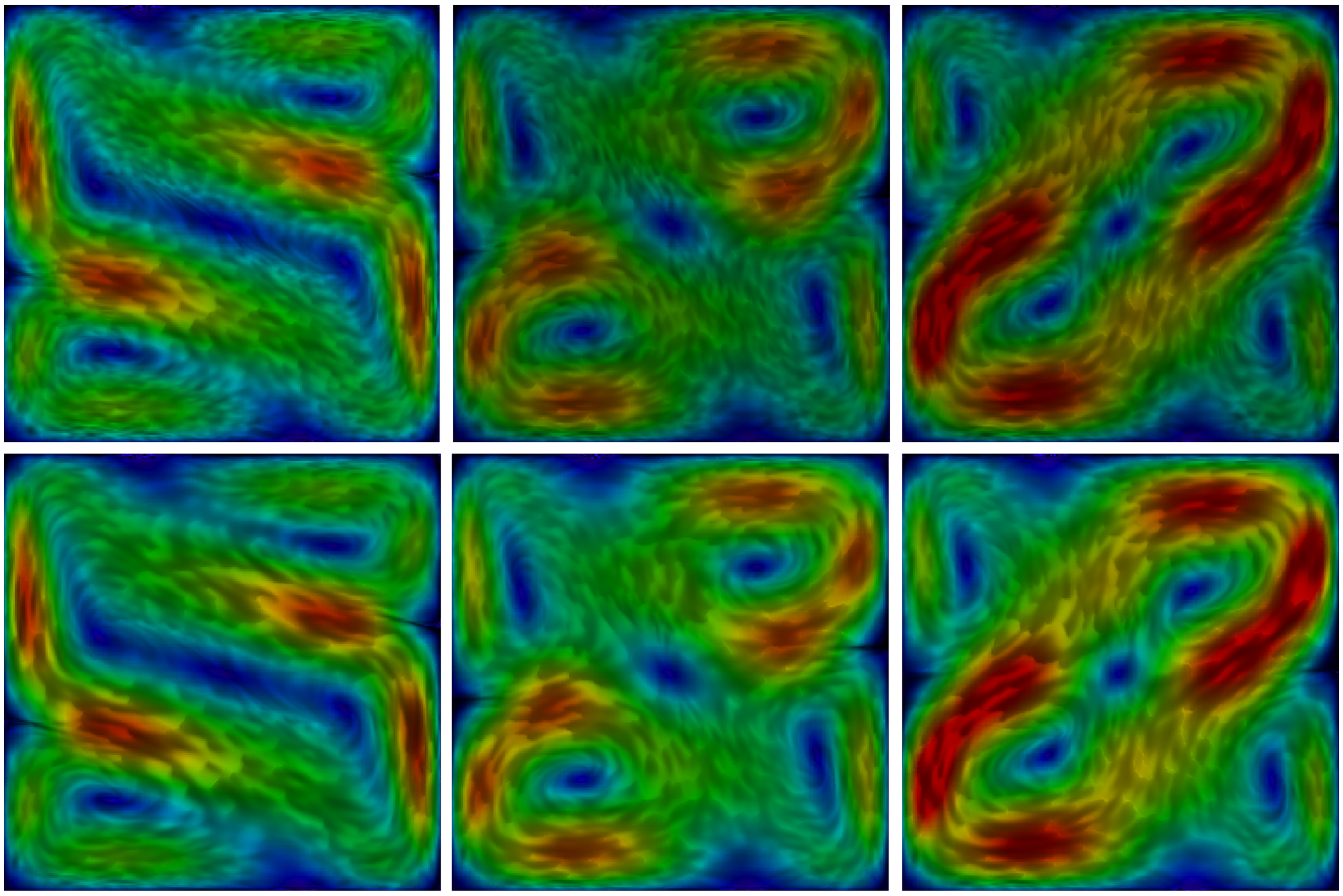

Figure 6: Three time-steps of the transport diffusion process of a Bénard convection, generating directed patterns. On the top row we consider a finer scale than on the bottom row. Color represents the velocity.

whose axes are the involved scale and time parameters. In detail we proceed as follows: First, we select a suitable interval for the scale parameter $[s_0, s_1]$ with $s_1 > s_0 > 0$ around our preferred multiscale resolution for the resulting images. Based on a smooth blending function $\psi : \mathbb{R} \to [0,1]$, vanishing outside $(-1,1)$, with $\psi(t) = \psi(-t) = 1 - \psi(1-t)$ for $t \in [0,1]$ and $\psi(0) = 1$, we can construct a partition of unity $\{\psi_i\}$ on the real line $\mathbb{R}$. I. e. we define $\psi_i(t) = \psi(\frac{2t-(i+1)(s_0+s_1)}{s_1-s_0})$. Now, for all $i = 0, 1, \cdots$ we separately solve the above transport diffusion problem for different starting times $t_i = i\,(\frac{s_1-s_0}{2})$ always considering some white noise of a fixed frequency range as initial data and denoting the resulting solution by ρ_i. For negative time we suppose a suitable extrapolation of the velocity field to be given. Finally, applying blending of at least two different solutions we compute

$$\rho(t,x) = \sum_i \psi_i(t)\rho_i(t,x)\,.$$

This intensity function is well defined for arbitrary times and characterized by the initially prescribed scale parameter interval. We especially use this construction for a animation of the flow over a certain time interval (cf. Fig. 8 for a graph of the blending functions). Such an animation involves all solutions ρ_i for which the blending function ψ_i has a nonvanishing overlap with the given time interval. Other constructions of a partition of unity and corresponding blending functions are near at hand and especially multiple overlaps can be considered which requires the blending of more than two intensity functions at the same time.

We emphasize that the application of this blending technique does not introduce any inaccuracy, because for any time t the resulting image $\rho(t,x)$ consists of images $\rho_i(t,x)$ showing streaklines at time t and at slightly varying scale.

The transport diffusion method creates a dense coverage of the domain with streakline patterns. These patterns are transported with the flow. Thus, this approach is capable of visualizing time dependent flow corresponding to streaklines of the same length as the evolving patterns. Since the evolving patterns are transported by the underlying flow this approach together with the blending technique discussed here is comparable to animated spot noise [5, 18].

8 Conclusions

We have generalized and expanded the anisotropic diffusion method in flow visualization for time-dependent vector fields. As a resulting continuous model we obtain a transport diffusion problem, where flow aligned patterns evolve under a dominating transport controlled by the vector field and an anisotropic diffusion process which stretches the patterns along the flow direction and sharpens them simultaneously in the perpendicular direction. This model can efficiently be discretized using an appropriate low viscous upwind scheme in time combined with a finite element scheme in space. For long-term animation purposes we select a suitable window for the involved scale parameter and use blending techniques to provide a dense pattern motion in the selected scale range at any time. As in the original method, most of the essential properties of the

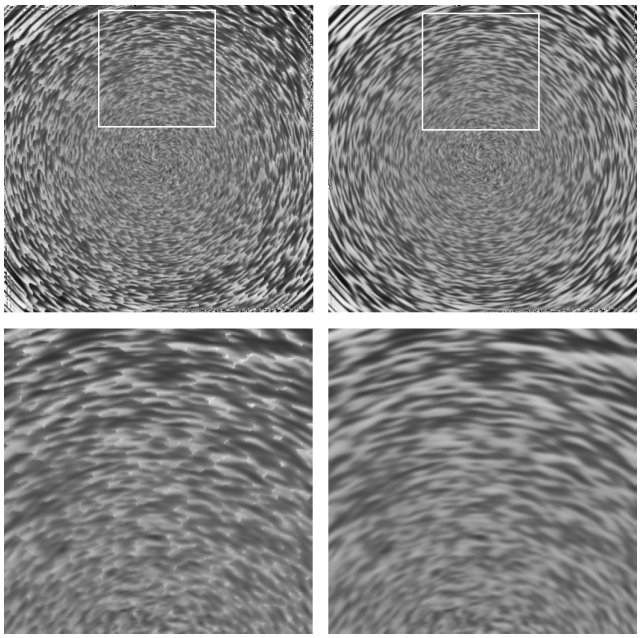

Figure 5: A comparison of directed and symmetric patterns generated for a circulating flow. On the left directed patterns are generated based on the incorporated "one–sided" diffusion and on the right the original model with linear diffusion along motions paths is depicted. The bottom row shows zoomed images of the marked regions in the top row.

model can be discussed based on the physically intuitive continuous model.

From the authors' point of view exciting future research directions are

- investigations of time-dependent flow visualization in 3D,
- combination of the flow visualization approaches with the accelerated solving strategies presented in [14] which will probably enable fast visualization also in 3D,
- the combination of this technique with other visualization methods to simultaneously display for instance chemical reactions in the moving fluid,
- an improved understanding of the nonlinear dependencies between the involved parameters.

Finally, we will work on a further improvement of the contrast enhancement and a better constrast preservation in the blending process.

On the web site

http://numerik.math.uni-duisburg.de/exports/flowVis/

different animations showing the performance and the underlying blending strategy are available.

Acknowledgements

We thank S. Turek from the University of Dortmund for his contribution to the efficient implementation of the public software and him and E. Bänsch from the Weierstraß-Institute at Berlin for providing the CFD data sets used in our computations.

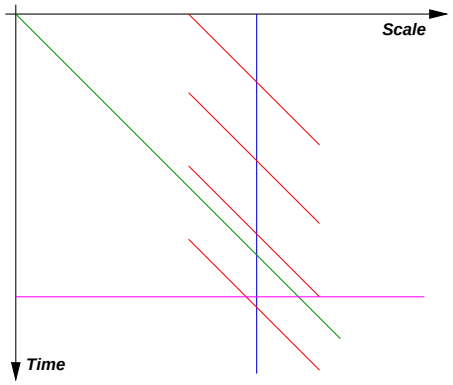

Figure 7: A schematic sketch of the general relation between scale and time parameter in our combination of image processing and flow computation is depicted. We compare the case of varying scale for steady state flow fields at fixed time (magenta), the simultaneously time and scale evolution (green), the optimal but non practical case of a fixed scale for varying time (blue) and our blending approach (red).

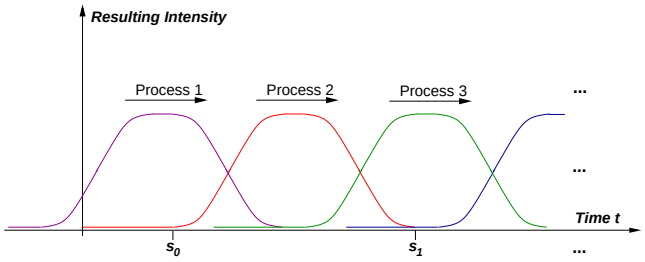

Figure 8: The weighting factors in the blending operation together with the overlapping scale/time intervals of the considered transport diffusion processes are shown in a diagram over time.

References

[1] L. Alvarez, F. Guichard, P.-L. Lions, and J.-M. Morel. Axioms and fundamental equations of image processing. *Arch. Ration. Mech. Anal.*, 123 (3):199–257, 1993.

[2] B. Kawohl and N. Kutev. Maximum and comparison principle for one-dimensional anisotropic diffusion. *Math. Ann.*, 311 (1):107–123, 1998.

[3] J. Becker and M. Rumpf. Visualization of time-dependent velocity fields by texture transport. In *Proceedings of the Eurographics Scientific Visualization Workshop '98*. Springer, 1998.

[4] B. Cabral and L. Leedom. Imaging vector fields using line integral convolution. In J. T. Kajiya, editor, *Computer Graphics (SIGGRAPH '93 Proceedings)*, volume 27, pages 263–272, Aug. 1993.

[5] W. C. de Leeuw and J. J. van Wijk. Enhanced spot noise for vector field visualization. In *Proceedings Visualization '95*, 1995.

[6] V. Interrante and C. Grosch. Stragegies for effectively visualizing 3D flow with volume LIC. In *Proceedings Visualization '97*, pages 285–292, 1997.

[7] J. Kačur and K. Mikula. Solution of nonlinear diffusion appearing in image smoothing and edge detection. *Appl. Numer. Math.*, 17 (1):47–59, 1995.

[8] N. Max and B. Becker. Flow visualization using moving textures. In *Proceedings of the ICASE/LaRC Symposium on Time Varying Data, NASA Conference Publication 3321*, pages 77–87, 1996.

[9] N. Max, R. Crawfis, and C. Grant. Visualizing 3D Velocity Fields Near Contour Surface. In *Proceedings of IEEE Visualization '94*, pages 248–254, 1994.

[10] P. Perona and J. Malik. Scale space and edge detection using anisotropic diffusion. In *IEEE Computer Society Workshop on Computer Vision*, 1987.

[11] P. Perona and J. Malik. Scale space and edge detection using anisotropic diffusion. *IEEE Trans. Pattern Anal. Mach. Intell.*, 12:629–639, 1990.

[12] Pironneau, O. *Methodes des elements finis pour les fluides.* Recherches en Mathematiques Appliquees., 7. Paris etc.: Masson, 199 p., 1988.

[13] T. Preußer and M. Rumpf. Anisotropic nonlinear diffusion in flow visualization. In *Proceedings Visualization 1999*, pages 325–332, 1999.

[14] M. Rumpf and R. Strzodka. Level set segmentation in graphics hardware. In *Proceedings ICIP'01*, 2001.

[15] H.-W. Shen and D. L. Kao. Uflic: A line integral convolution algorithm for visualizing unsteady flows. In *Proceedings Visualization '97*, pages 317–322, 1997.

[16] D. Stalling and H.-C. Hege. Fast and resolution independent line integral convolution. In *SIGGRAPH 95 Conference Proceedings*, pages 249–256. ACM SIGGRAPH, Addison Wesley, Aug. 1995.

[17] J. J. van Wijk. Spot noise-texture synthesis for data visualization. In T. W. Sederberg, editor, *Computer Graphics (SIGGRAPH '91 Proceedings)*, volume 25, pages 309–318, July 1991.

[18] J. J. van Wijk. Flow visualization with surface particles. *IEEE Computer Graphics and Applications*, 13(4):18–24, July 1993.

[19] J. Weickert. *Anisotropic diffusion in image processing.* Teubner, 1998.

[20] D. Weinstein, G. Kindlmann, and E. Lundberg. Tensorlines: Advection-diffusion based propagation through diffusion tensor fields. In *IEEE Visualization 1999*, pages 249–253, 1999.